Chapter 4

Automated Cell Separation Techniques Based on Optical Trapping

T. N. Buican

Life Sciences Division, Los Alamos National Laboratory, Los Alamos, NM 87545

Optical trapping can be used to levitate and manipulate a wide variety of microscopic particles, including living cells and chromosomes in aqueous suspension. Both two-dimensional (2-D) and three-dimensional (3-D) optical traps can be easily produced and can be used, respectively, for sorting and manipulating microscopic particles. We describe two cell separation techniques developed in our laboratory: (1) laser sorting, based on the use of 2-D traps; and (2) microrobotic manipulation, which uses a 3-D optical trap, video microscopy and machine vision in order to separate single cells and chromosomes. Both techniques can be integrated into complex instruments for the analysis, separation, manipulation and processing of individual cells and cell organelles.

Optical trapping, a purely optical technique for the manipulation of microscopic particles, was invented in the late '60s by Arthur Ashkin of AT&T Bell Labs (*1*). The technique relies on the pressure created by one or more laser beams that are scattered by a microscopic object in order to trap, levitate, and move that object. As opposed to other trapping techniques, optical traps are intrinsically stable and very localized in their effects. As such, they can be incorporated into relatively simple devices that allow single cells, chromosomes, and other cell organelles to be accurately positioned and transported. Furthermore, optical trapping only requires low-intensity laser beams and can be operated at wavelengths at which absorption by the trapped particle is minimized. Thus, for most cells that have been optically trapped, the trapping laser beams seem to have negligible biological effects (*2-4*).

Cell separation based on optical trapping belongs to the class of *active, single-cell* sorting techniques, together with flow sorting and mechanical micromanipulation. As such, automated optical trapping instruments analyze single cells and, after converting the measurement results into a sorting decision, physically remove selected single cells from the original sample. Although passive cell separation based on optical trapping has also been proposed (*5*), the complex dependence of separation properties on the physical properties of the cell and the existence of beam-mediated interactions between cells (*6*) make this technique unattractive. By contrast, active separation based on optical measurements of single-cell prop

0097–6156/91/0464–0059$06.00/0

erties and automated beam control can be very precise both in terms of its analysis of single cells and in the physical separation of these cells. Furthermore, automation applies in a natural way to optical trapping as the trapping optics can easily be used for light collection and imaging, and the direction and intensity of the laser beams used for trapping can easily be brought under automated control.

The range of cell properties on which automated cell separation can be based in an optical trapping system includes labelling fluorescence intensity, light scattering intensity distribution, and cell morphology. As the speed at which cells travel through the analysis volume can be accurately controlled and is much lower than the typical speeds encountered in flow sorting, high-resolution measurements of cell properties can be made. Furthermore, since cell position can be controlled with very high accuracy, other, nonoptical measurements can be performed.

The purely optical nature of cell manipulation by optical trapping means that cell analysis and manipulation can be performed inside *completely enclosed* sample systems. Thus, separation based on optical trapping has a clear advantage over mechanical micromanipulation, which can only be performed in open containers. The small diameter of the trapping beams and the highly localized character of the optical trap allow manipulation to be performed inside commensurately small compartments. Consequently, a single optical manipulation chamber can contain a large number of compartments and interconnecting channels. The former can be used not only for collecting cells that have been separated, but also for performing further analysis and processing of those cells. Thus, complex experimental protocols can be carried out at the level of the single cell inside an optical manipulator, without the need for recovering the cells after each step and transporting them between separate instruments.

We begin this article with a brief presentation of the principles of optical trapping. Following this, we discuss the applications of two-dimensional (2-D) and three-dimensional (3-D) optical traps in cell separation. For each type of trap we discuss instrument optics, manipulation chambers, control electronics, and the procedures for automated control. We conclude with a brief discussion of future developments in the field of cell separation and processing by optical trapping.

A Qualitative Discussion of Optical Trapping

Whenever light is scattered by an object, the change in the momentum of the scattered photons leads to a momentum of equal magnitude but opposite direction being transferred to the scattering object. If one considers a system consisting of a scattering object and the incident and scattered beams (Figure 1), and if P_0 and P_1 are, respectively, the momentum fluxes (momentum transported by the beams per unit time) of the incident and scattered beams, then, because of conservation of total momentum, a force, $F = P_1 - P_0$, is produced that acts on the scattering object. This is the *radiation pressure force*, and we will refer in what follows to its components along the direction of the incident beam (axial force) and perpendicular to that direction (radial force).

The momentum carried by a light beam in a given direction can be computed from the far-field angular distribution of the beam intensity, ρ, and is described by

$$P = \frac{W}{c} \int_{4\pi} \rho \cos\alpha \, d\Omega$$

where W is the total beam power, c is the speed of light, α is the angle relative to the given direction, and $d\Omega$ is the solid angle element (*7*). For an axially symmetric beam, the factor, $\cos\alpha$, shows that, at constant total beam power, beam mo-

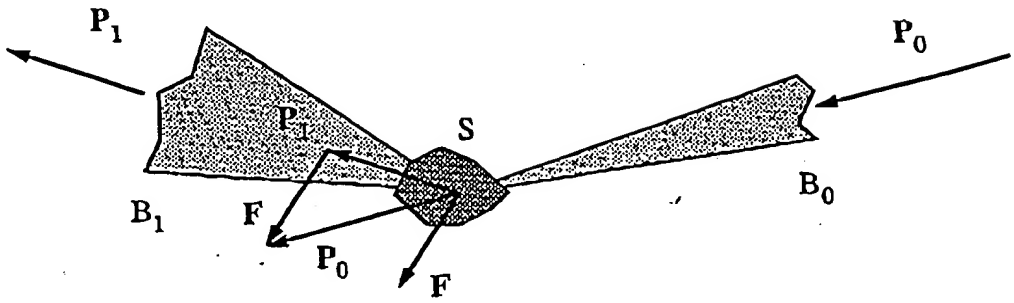

Figure 1. Conservation of momentum in a light scattering system: B_0, B_1—incident and scattered beams; S—scattering object; P_0, P_1—momentum fluxes of the two beams; F—light pressure force due to scattering of the incident beam by S.

mentum decreases as the divergence of the beam increases. It follows immediately that beam momentum is decreased by (i) absorption (which reduces beam power); and (ii) diffuse scattering (which spreads out the intensity distribution). Absorption produces a purely axial force in the direction of the incident beam. Diffuse scattering, if symmetric relative to the direction of the incident beam, also contributes a force in the direction of the incident beam.

It can be shown that the momentum flux of a beam with axial symmetry is parallel to the beam axis and has a magnitude given, for small θ, by $P = W (1 - \theta^2) /c$, where θ is an angular parameter describing beam divergence. This relationship shows that the beam has maximum momentum when it is maximally collimated ($\theta = 0$), and its momentum decreases as its divergence increases. The magnitude of the force acting on the scattering particle is thus given by $F = - W \Delta(\theta^2) / c$. If the scattering object behaves like a lens or mirror, the beam angle, θ, can either increase or decrease, depending on the geometry of the object and incident beam. Consequently, we may expect both the magnitude and direction of the light pressure force acting on an optical element to depend on the optical properties of the object, as well as its position relative to the incident beam.

The Lens Model. Under most experimental conditions, live cells have a refractive index close to that of the suspension medium (δ) and, therefore, at least in a first approximation, partial reflection does not play an important role in biological optical trapping. An adequate qualitative description of the optical trapping of biological particles can thus be obtained by treating the particles as lenses that refract the incident beam.

Radial Trapping. It is easy to see that, whenever an object that behave like a convergent lens (internal index of refraction higher than that of the sur rounding medium) is moved away from the axis of a light beam incident on it, th light beam is deflected away from the initial direction (Figure 2a). Therefore, th radial component of the light pressure force acting on the object points in a direc tion opposite to particle displacement (toward the beam axis), and a stable, 2-I trapping effect is created. One can similarly show that the radial force acting on divergent lens (object with a lower refractive index than that of the mediun points in the same direction as the displacement (Figure 2b) and thus there is r radial trapping effect. Radial trapping applies to both spherical and nonspheric

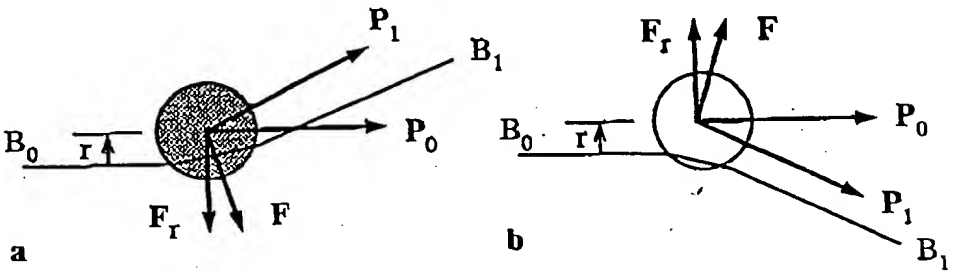

Figure 2. The orientation of the radial force: (a) particle with higher refractive index than that of the surrounding medium; and (b) particle with lower refractive index. B_0, B_1—incident and scattered beams; F—light pressure force; F_r—radial component of F; P_0, P_1—momentum fluxes for the incident and scattered beams; r—radial particle displacement. Only the axes of the beams are shown.

particles. In the case of the latter, torques may develop which give the particles preferential orientations relative to the incident beam.

Axial Trapping. In the lens model of optical trapping, the particle in the laser beam is regarded as a lens of focal length, f (Figure 3). In a purely geometrical optics approximation, one can easily see that there are always two points along the beam axis for which the angle of the output ("scattered") beam equals that of the

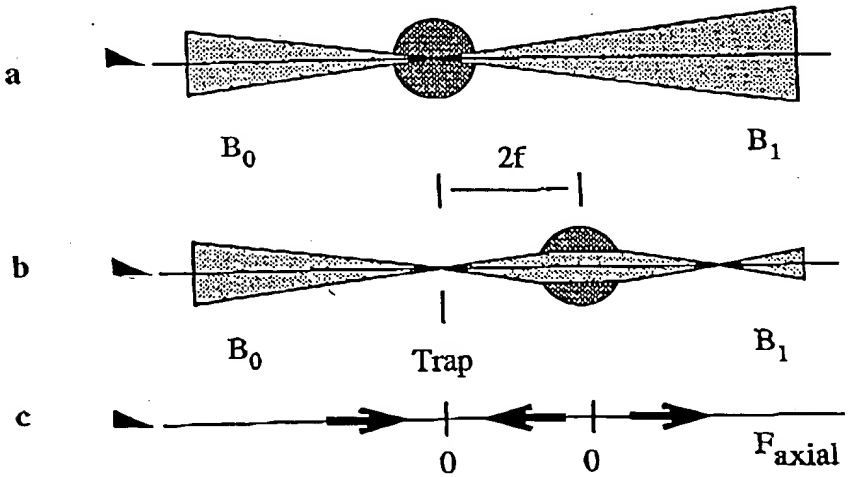

Figure 3. Lens model of optical trapping. Two particle positions for which the axial force vanishes: (a) particle at beam focus; (b) particle at a distance 2f from the beam focus; (c) diagram showing the direction of the axial force (F_{axial}) for various positions of the particle. The position of the stable axial trap relative to the trapping beam is indicated. The focal length of the particle is denoted by f. The incident and scattered beams, B_0 and B_1, travel from left to right.

incident beam. Thus, the momentum fluxes of the two beams have the same magnitude and, for distances of 0 and 2f between the lens and the beam focus, the axial force vanishes (Figure 3c). It is also easy to see that, for any distance between 0 and 2f, the beam angle decreases after passing through the object and, therefore, the beam momentum increases and the light pressure force acting on the lens is directed opposite to the beam. For all points outside this interval, the beam mo-

mentum decreases and the lens is pushed in the direction of the beam. As a consequence of this dependence of the axial force on the distance between lens (object) and beam focus, a stable axial trap always exists in a purely geometrical optics model and is situated at the beam focus. However, if one considers a Gaussian beam and the corresponding imaging relationships (*9*), one can show that an axial trap exists only if $\theta^2 > \lambda/\pi f$, where λ is the wavelength and θ is the asymptotic angle of the Gaussian beam (*9*). Thus, for weakly convergent beams (small θ), the inequality above is not satisfied. Consequently, the axial force always points in the direction of the beam and there is no axial trapping. One can thus define two trapping regimes, depending on the degree of convergence of the beam: (i) 2-D trapping, which applies to weakly convergent beams and in which there is a trapping effect only in a plane perpendicular to the axis of the trapping beam; and (ii) 3-D trapping, in which a strongly convergent laser beam creates a full, 3-D optical trap.

2-D Optical Trapping and Cell Separation

We showed in the previous section that weakly collimated laser beams produce 2-D optical traps and that trapped particles are propelled along the beam axis. Such traps may be used to transport microscopic particles over macroscopic distances and can thus be the basis for both remote delivery and sorting systems.

As the particles in a 2-D trap move along the beam axis, hydrodynamic forces which depend on particle shape and size will affect both the velocity at which the particles travel and the stability of the trapping effect. Thus, during the 2-D trapping of blood cells, we observed that lymphocytes, which are roughly spherical, are stably trapped and can be transported over relatively large distances (*6*). By contrast, erythrocytes are only briefly held in the beam and are readily pushed out by orientation-dependent hydrodynamic forces. This phenomenon could be used for the passive separation of spherical from nonspherical cells.

The velocity at which stably trapped cells travel along weakly focused beams depends on both the optical and the hydrodynamic properties of the cells. The use of differences in travel velocity for passive cell separation has been proposed by Ashkin (*5*). However, the travel velocity of a given particle is further affected by the scattering of the beam by closely following, trapped particles. We have reported (*6*) that the interaction between simultaneously trapped particles may lead to the formation either of particle clumps or of stable systems of particles which move at the same velocity while maintaining a constant separation. In either case, passive separation is no longer possible, as travel velocity now depends on the properties of more than one cell. The simultaneous presence of several particles in the trapping beam can be avoided by lowering the rate of particle injection and thus limiting the throughput of any passive sorting system of this kind.

The use of weakly focused laser beams to transport, rather than sort, microscopic particles has the important advantage that proper alignment of the transportation beam with the collection volume is sufficient to ensure precise delivery of the trapped particles. Thus, a transportation system based on a weakly collimated beam requires minimal adjustment. Furthermore, such a system can accurately deliver microscopic particles through apertures with diameters comparable with the diameter of the trapping beams, and can thus move selected particles between separate compartments in a complex, integrated instrument.

Laser Sorting. The macroscopic transportation capabilities of weakly focused laser beams can be used for the automated sorting of microscopic particles. A particle travelling along a weakly focused beam can be transferred to another, intersecting beam, provided the intensity of the latter is above a threshold value that depends on the intensity of the first beam and the relative positions of the bear

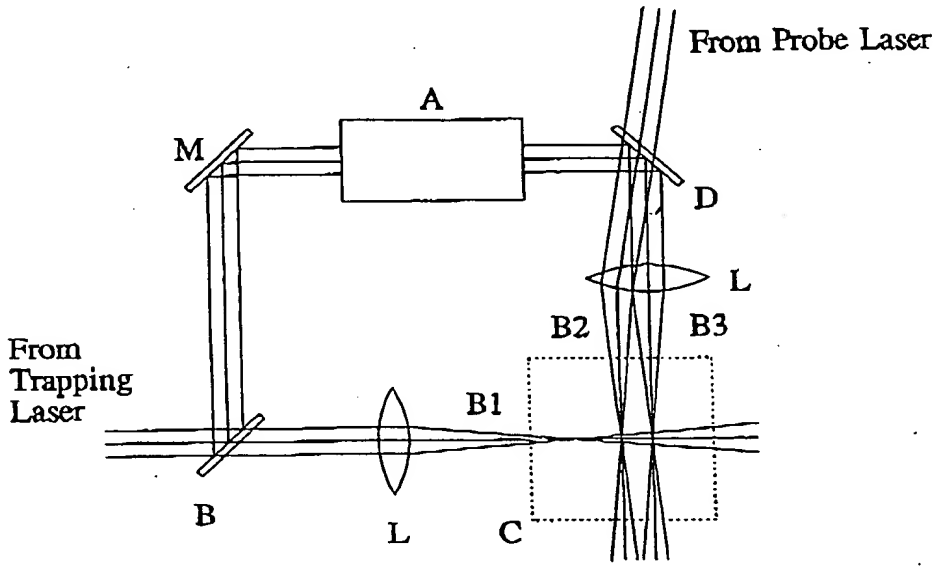

Figure 4. Simplified diagram of the laser sorter optics: A—acoustooptic modulator; B—beam splitter; B1—propulsion beam; B2—probe beam; B3—deflection beam; C—manipulation chamber; D—dichroic mirror; L—focusing lenses; M—mirror. The light collection optics are not shown.

waists. Intersecting beams can thus be used to direct trapped particles to one of several collection volumes. An automated sorting system based on light scattering measurements is described in (*6*) and a diagram of the instrument optics is shown in Figure 4. Naturally, other optical, as well as nonoptical, parameters can be used to control sorting. A manipulation chamber for laser sorting (*6*) is shown in Figure 5. Channels machined into the top of the chamber are enclosed by a window that allows the particles in the chamber to be visualized. Light scatter measurements are also made through this window. The laser beams enter the channels through side windows, and the sample is injected into the propulsion beam through a sample port. There are two ports just ahead of each side window that are used to create localized fluid flows. Individual cells are trapped in the propulsion beam and start travelling along its axis. As each cell intersects the probe beam (of wavelength different from that of the trapping beams and of lower inten-

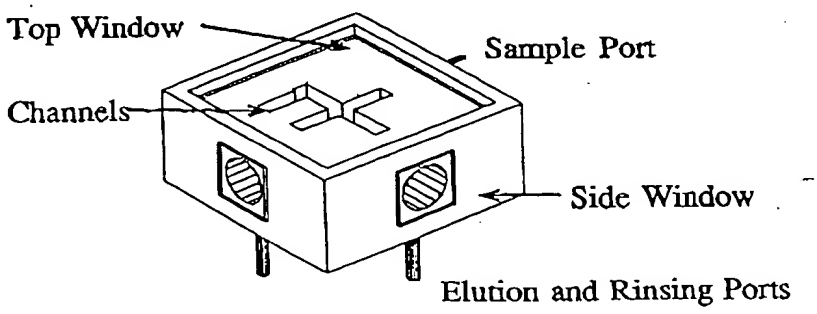

Figure 5. View of the laser sorter manipulation chamber (see Figure 4 for the geometry of the beams inside the chamber). The side windows allow the three laser beams to enter and exit the chamber. The elution and rinsing ports are used to create local fluid flows near the side windows.

sity), the scattered light intensity is measured and a sorting decision is made. When a cell reaches the deflection beam (typically about 100 μm downstream from the probe beam), the intensity of this beam is modified by an acoustooptic modulator so as to direct the particle to the appropriate elution volume. Localized fluid flows just ahead of the beam output windows are used to elute the cells.

The beam focusing optics on the laser sorter described in (*6*) had a focal length of 50 mm. At a power of approximately 300 mW per beam, typical particle velocities reached several hundred μm/s. For a separation between probe and deflection beams of 100 μm, this resulted in a maximum sorting frequency of a few cells per second. Although this rate is too low to make the instrument a practical sorter, its simplicity and the relatively large distances travelled by the cells (over 6 mm) may allow a similar system to be used as a microscopic gating device that prevents unwanted cells from drifting through narrow apertures connecting the compartments of an integrated analysis and preparation instrument, while letting through selected cells.

The elements of the sorting control system are shown in Figure 6. The light

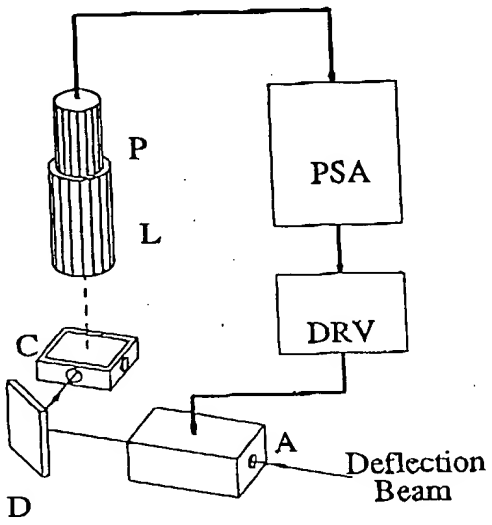

Figure 6. Automated control of the laser sorter: A—acoustooptic modulator; C—manipulation chamber; D—dichroic mirror; DRV—modulator driver; PSA—pulse shape analyzer; L—lens; P—photomultiplier. The dashed line represents the light collection path, while the wide, solid line represents the signal and control path. The deflection beam focusing lens is not shown.

scattered by each cell as it passes through the probe beam is collected by a le and falls on a photomultiplier. The pulse produced by the detector is analyzed by pulse shape analyzer and a sorting decision is made on the basis of the propert of this pulse.

The parameter of choice for controlling the laser sorter is pulse amplitu Pulse area, which is a commonly used sort control parameter in flow sorters, not suitable for controlling laser sorting because pulse widths are not const This is due to the fact that particle velocity in the propulsion beam depends many particle properties and is also affected by the presence of other particles the beam (*6*).

Secondary parameters, such as pulse width and time interval between pul are also derived by the pulse shape analyzer. These parameters, the values which can indicate a separation between successive particles too small to al individual analysis and/or separation, are used to disable deflection and thus a compromising sort purity.

Microrobotic Manipulation

A different approach to cell separation is made possible by the use of a 3-D optical trap. While the laser sorter is operationally equivalent to a flow sorter (in the sense that it separates cells into a small number of collection volumes and that measurements are performed on particles moving along a well-defined axis), the 3-D optical trap can be used for microscopic robotic manipulation of single cells and cell organelles. This technique is well suited for the automated separation of rare cells and can also be easily integrated into complex instruments.

Optical Manipulator Designs. Two basic optical manipulator designs, both originating in Ashkin's work (*1*, *10*), have been proposed and implemented. The two designs differ in the number of laser beams used to produce a 3-D optical trap (Figure 7). The single-beam optical manipulator (Figure 7a) relies upon the use

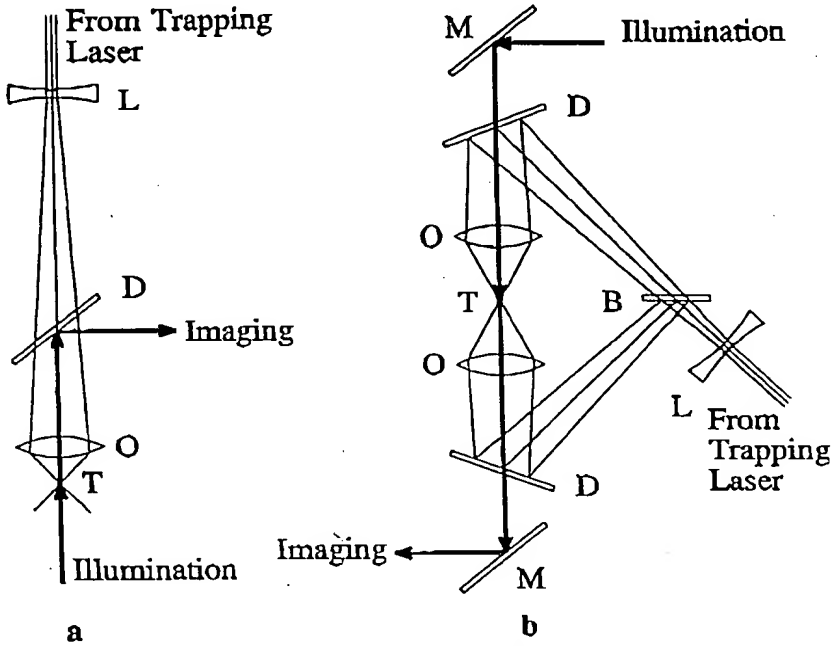

Figure 7. Simplified diagram of single-beam (a) and double-beam (b) optical trapping and imaging systems. B—beam splitter; D—dichroic mirror; L—divergent lens; M—mirror; O—microscope objective; T—optical trap. The arrows represent the imaging optical paths.

of a high numerical aperture focusing lens and has been implemented on commercial microscopes (*10*). The double-beam system (Figure 7b) uses lower numerical aperture lenses, and a stable 3-D trap is produced by two coaxial, counterpropagating beams (*11*). In both cases, the lenses used for focusing the trapping beam(s) are also used for imaging, and dichroic mirrors are used to separate the trapping and imaging wavelengths.

The single beam optical trap illustrated in Figure 7a can be implemented on any microscope with only minor modifications to the microscope optics. The illumination source is the microscope condenser, while imaging is done through the existing microscope optics. The role of the additional divergent lens is to expand the trapping laser beam in order to fill the input aperture of the microscope objective and thus maximize the convergence of the trapping beam. The position of the trap within the field of view of the microscope can be modified by moving the divergent

lens (*3*). Longer-range motion of the trap can be achieved by moving the manipulation chamber relative to the trapping beam. A variant of Ashkin's single-beam design was proposed in (*12*), where an optical trap was added to a confocal microscope by means of a second microscope objective. The second objective, which is used exclusively for trapping, is mounted on an xyz stage and can thus control the position of the optical trap.

The trapping beams in the double-beam system are derived from a single laser beam by means of a beam splitter. The use of a divergent lens for beam expansion is optional, as a high degree of convergence of the trapping beams is no longer critical in this system. The optics for this type of manipulator are more complex than those of the Ashkin design and attention must be paid to the proper alignment of the trapping beams. However, beam alignment can be monitored by a video camera that images the beams after a complete round trip through the system and can thus be automated (*11*).

Because of their different optical characteristics, the two optical manipulator designs have different applications. The single-beam manipulator, which uses a high numerical aperture lens, is capable of high-resolution imaging and can produce small-diameter, high-intensity traps. This manipulator is therefore most suitable for the analysis and manipulation of small particles such as cell organelles. At the same time, the use of a high numerical aperture lens leads to a small field of view and a very small working distance. The small field of view restricts the use of such a manipulator in an automated separation system, where the performance of automated navigation algorithms depends to a large extent on the size of the field of view. Furthermore, the very small working distance makes difficult the use of complex manipulation chambers.

By contrast, the dual beam system provides lower-resolution imaging but has a wider field of view and larger working distance. This system is eminently suited for automated cell and chromosome separation. In applications such as chromosome separation, the lower resolution of the images provided by the double beam manipulator can be compensated for through the use of specific fluorescent probes. The large working distance which, for modern ultralong working distance objectives, can be around 1 cm, allows the optical manipulator to be easily integrated into complex systems.

Optical Manipulation Chamber Designs. Optical manipulation chambers may incorporate features that facilitate cell separation. For instance, multiple compartments inside the chamber allow selected cells to be physically separated from the original cell sample. It is also desirable for the manipulation chamber to have ports through which the sample can be introduced and the separated cells can be eluted. If the chamber has multiple compartments, then it is preferable for each compartment to be connected to separate external ports. Finally, if the cell sample is highly concentrated (as is the case, for example, with blood samples), it is desirable for the manipulation chamber to be shallow. Low chamber depth ensures that, after sedimentation of the cells, the surface concentration is sufficiently low to permit the trapping and removal of single cells.

Manual cell separation through optical manipulation was demonstrated by Ashkin (*3*) in a rather crude chamber that contained a hollow, transparent fiber We described a multicompartment chamber design (*11*) that is well suited for cel separation, while also containing features that make it attractive for complex worl with live cells. This chamber (Figure 8) consists of three layers that are cemente together. The outer layers are good quality glass of 170-μm and 1-mm thickne respectively. The central layer, which contains the pattern of compartments an channels, can be fabricated either from stainless steel shim stock or from a phot sensitive ceramic (Fotoceram, Corning). Small compartments and channels can l accurately cut through the central layer by laser machining (stainless steel)

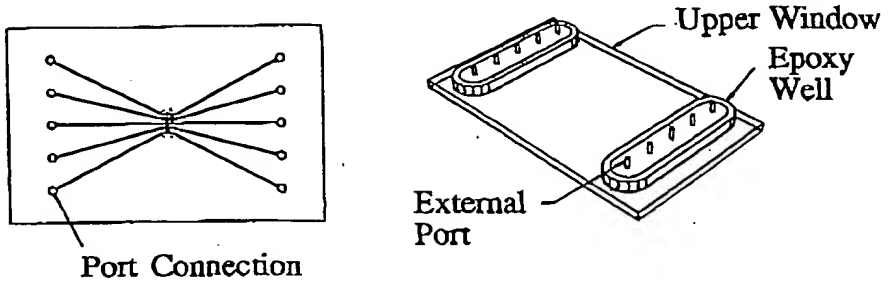

Figure 8. Multicompartment manipulation chamber: (a) Top view of the central layer, showing compartments (central region) and interconnecting channels; and (b) perspective view of the upper window, showing the external ports.

photoetching (Fotoceram). A view of the central section is shown in Figure 8a, where one can see five compartments (300 μm by 300 μm) and channels connecting the compartments with each other and with the external ports. The external ports are connected to internal channels through holes in the 1-mm-thick glass window, to which they are cemented (Figure 8b). The small thickness and large surface area of this manipulation chamber lead to efficient heat exchange and temperature control. This characteristic is particularly important when separating and processing live cells, as well as for performing biochemical assays inside the chamber. Furthermore, the channels connecting each compartment to external ports allow reagents and culture media to be circulated through the compartments, and complex, long-term protocols can thus be carried out inside the chamber.

Automated Control Based on Machine Vision. The ability of optical manipulators to image and manipulate single cells makes this type of instrument amenable to machine-vision-based automation. The control problem in such an instrument consists of the following: (i) finding the cells of interest; and (ii) separating those cells without collecting unwanted particles. In order to simplify image acquisition, we assume that the particles injected into the chamber have been allowed to settle onto the bottom window. Obviously, a shallow chamber has the advantage that particle settling occurs quickly and the delay between sample injection and the beginning of the search procedure is short. The search procedure consists of scanning through the sample and analyzing each particle in the instrument's field of view. Once a cell of interest has been identified, it is trapped and raised to a certain height above the bottom window (Figure 9), following which it is transported to an area where it is either recovered or further analyzed and processed.

Given the initial position of the trapped cell and the coordinates of the target position, separation must proceed along a path that does not collide either with the chamber walls or with unwanted particles. For a simple chamber consisting of a single, convex compartment, the first requirement is easily satisfied. The simplest path satisfying the second requirement depends on the depth of the chamber. As optical traps are generally better localized in a plane perpendicular to the trapping beams than along the beam axis, a shallow chamber may require the trap to be moved around unwanted particles in order to avoid trapping them. This is illustrated in Figure 9, where we distinguish between the *separation path* followed by the trap, and the *clear path*, which is the projection of the former onto the bottom

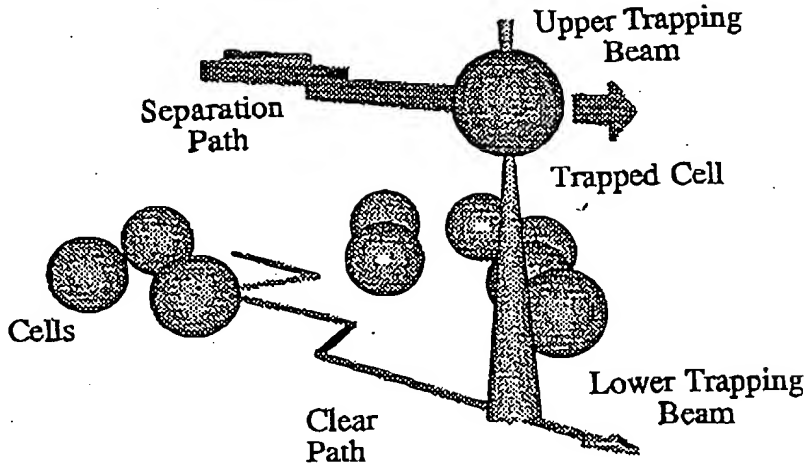

Figure 9. Geometry of cell separation by optical manipulation. The trapped cell is carried along a separation path that avoids other cells on the bottom of the manipulation chamber. The cells in the chamber are imaged along the common axis of the trapping beams. The clear path, which is the projection of the separation path onto the bottom of the chamber, is constructed so as to avoid the trapping of unwanted cells.

of the chamber. Finding a clear path from a knowledge of the positions and sizes of the settled cells is the classical collision avoidance problem of robotics. In the case of an optical manipulator, a clear path must be computed gradually, on the basis of a succession of overlapping video frames (Figure 10). This will be discussed in more detail in the next section. Automated navigation is not required for chambers that are deeper than the axial dimension of the trap, and the separation path is, consequently, a straight line at a height above the bottom window that is sufficient to prevent the trapping of unwanted cells.

The computation of the separation path is slightly more complicated for a multicompartment chamber, where the trap must avoid not only other cells, but also the edges of compartments and channels. In this case, a rough path that avoids collision with chamber edges may have to be computed first, following which the rough path is used to define the local direction of motion followed by the clear path (Figure 10). The rough path can be easily computed from a stored map of the manipulation chamber (*11*).

Single Video Frame Navigation. The automated navigator that controls cell separation by optical manipulation must find a clear path within the boundary of the current field of view, such that (i) it avoids collision with particles on the bottom of the chamber; and (ii) it leads, as closely as possible, in the direction defined by the rough path. Once such a path has been found for the current field of view, the instrument moves the optical trap and the trapped particle along the clear path to a point close to the edge of the video frame (Figure 10). Following this, a new video frame is acquired and the process is repeated until the target position is reached.

A wide variety of algorithms for finding collision-free, clear paths have been constructed (*13*). We have developed a navigator algorithm that is derived from the circle tangency techniques described in (*14*). This type of navigator algorithm, which approximates objects by circles of appropriate radius, is computationally efficient and is well suited for the usual cell shapes. The circle tangency algori

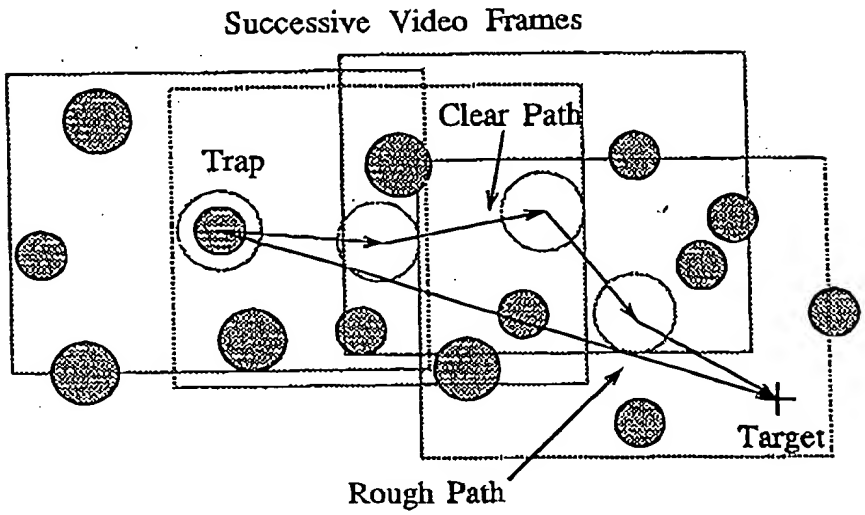

Figure 10. Automated navigation for robotic particle separation: Computation of a collision-free, clear path through a succession of overlapping video frames. The point labelled "Target" is, depending on the location of the trap along the rough path, either the next vertex of the latter, or the final target position.

constructs a clear path that consists of arcs along circular object boundaries and line segments that are tangent to the boundary of the last encountered object and point in the direction of the current target point. If the target point is not in the current video frame, all clear paths leading to the frame boundary are computed, together with weights that increase with path length and deviation from the direction leading directly to the target. The path with the lowest weight is chosen, the trap is moved to the point on the path within a trap radius of the boundary, a new video frame is grabbed, and the process is repeated until the target position is reached.

The navigator algorithm stores the position and size of all previously detected objects and uses this information when computing a path. This ensures that no path is chosen that leads to a previously detected object that lies beyond the boundary of the current frame. The algorithm can also move back along a path if it finds itself inside a cul-de-sac. The algorithm monitors the continued presence of a particle inside the trap and alerts the operator if the particle is lost.

The example in Figure 11 illustrates the operation of the automated navigator and shows the ability of the algorithm to use previously acquired information. The diagrams are printouts of the image display area of the user interface screen, showing polystyrene microspheres with a diameter of 5.8 μm. The x, y coordinates (in μm) of the optical trap and of the field of view are shown, respectively, near the bottom and left sides of the images. The rough path, shown in Figure 11a, intersects particle 2. The navigator algorithm computes clear paths within the current video frame and chooses the path shown in Figure 11b as having the smallest angular deviation from the rough path (the clear path extends from the trap to the stopping point, S). The position information for the other particles in the frame is stored. As the trap is moved to the stopping point of Figure 11b, a new frame is grabbed (Figure 11c). A new computation of the clear paths is performed, and the navigator reverses direction by using the previously stored information about the position of particle 1 (Figure 11d). The trap is successfully moved around particle 1 (Figure 11e), and the target is reached in Figure 11f.

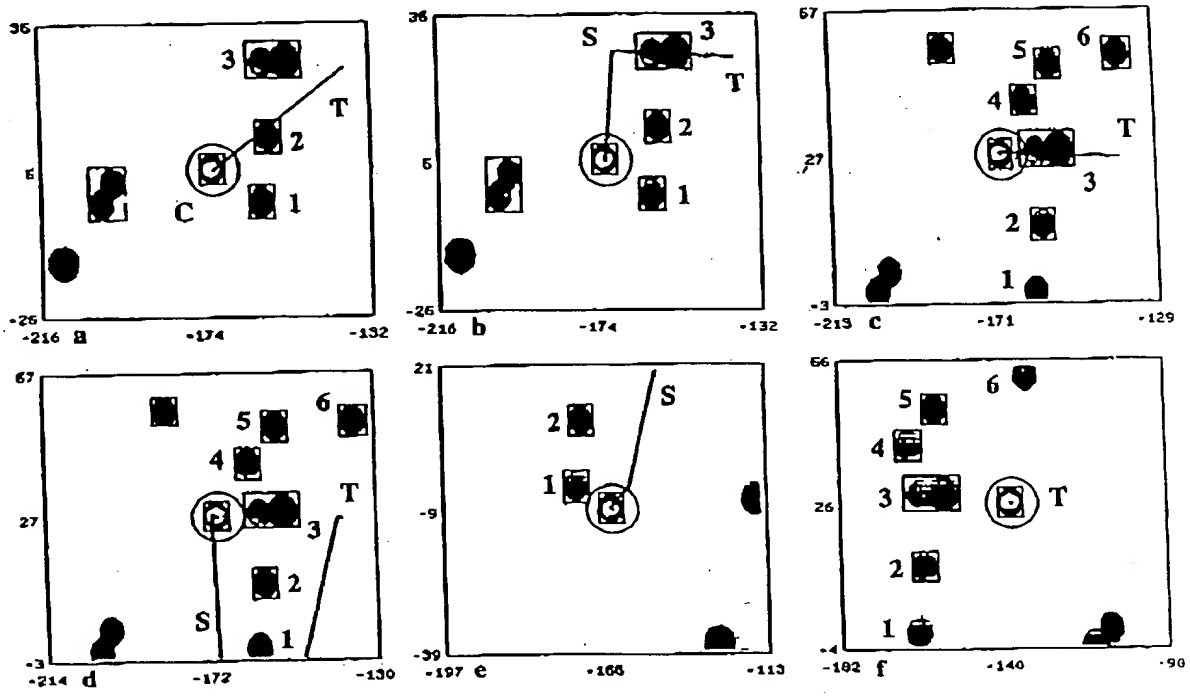

Figure 11. Automated navigation of the optical trap. The binary images show polystyrene microspheres with a diameter of 5.8 μm. One particle is held in the optical trap (central circle). The trapped particle must be moved without collision from the current position, C, to the target point, T. C—current trap position; S—stopping point; T—target position; 1-6—obstacles.

Automated Control System. The main elements of the control system for microrobotic cell separation are shown in Figure 12. The imaging system, which is no more than a video microscope, provides a video signal which is digitized by a frame grabber and made available to a processor. The processor performs a series

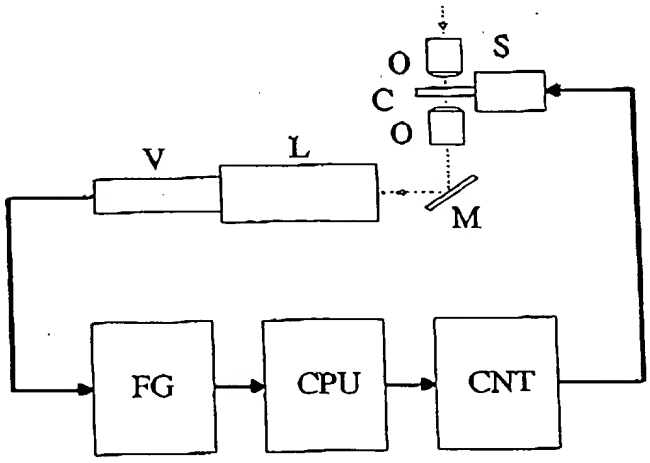

Figure 12. Automated control of the optical manipulator: C—manipulation chamber; CNT—servo controller; CPU—central processing unit; FG—frame grabber; L—imaging lens; M—mirror; O—microscope objective; V—video camera; S—xyz stage with servo actuators. The dotted line represents the imaging optical path, while the solid line represents the data and control path.

of operations on the digitized video frame which lead to the computation of a local clear path. Once the clear path for the current frame has been computed, the processor downloads the coordinates of the path vertices to a servo controller, and the servo actuators on an xyz stage move the manipulation chamber accordingly.

Given the computation-intensive nature of the image processing and machine vision algorithms, it is obvious that the speed at which cells can be separated depends, to a large extent, on the computing power available for controlling the optical manipulator. As shown in Figure 12, the robotic manipulator described in (*11*) uses a single processor both for running the image analysis and machine vision algorithms, and for controlling the relative position of the optical trap. Furthermore, the same processor operates the rest of the hardware, as well as a high-resolution, interactive user interface. Consequently, separation of trapped cells does not proceed at the maximum possible speed, which is only limited by viscous drag and beam intensity. The data processing bottleneck can be overcome by using real-time, multiprocessor systems, which are now available at reasonable cost.

Conclusions

The manipulation techniques made possible by optical trapping are well suited for large-scale automation and integration. As such, they have the potential to provide the technological basis for complex, powerful, and efficient "microscopic laboratories" for cell biology, cytogenetics, and molecular biology. Such instruments would perform complex analytical and preparative procedures on single cells and chromosomes, while requiring a minimum of human intervention. This approach may open up new avenues in experimental biology and biotechnology.

Acknowledgments

The automated navigator software was written by Bryan D. Upham. This work was supported in part by LANL ISRD Award X86C, NASA contract T-1196P, and by the National Flow Cytometry Resource (grant RR01315).

Literature Cited

1. Ashkin, A. *Phys. Rev. Lett.* **1970,** *24,* pp. 156-159.
2. Ashkin, A.; Dziedzic, J. M. *Science* **1987,** *235,* pp. 1517-1520.
3. Ashkin, A.; Dziedzic, J. M.; Yamane, T. *Nature* **1987,** *330,* pp. 769-771.
4. Block, S. M.; Blair, D. F.; Berg, H. C. *Nature,* **1989,** *338,* pp. 514-518.
5. Ashkin, A. *U. S. Patent No. 3,710,279,* 1973.
6. Buican, T. N.; Smyth, M. J.; Crissman, H. A.; Salzman, G. C.; Stewart, C. C; Martin, J. C. *Appl. Opt.* **1987,** *26,* pp. 5311-5316.
7. Bohren, C. F.; Huffman, D. R. *Absorption and Scattering of Light by Small Particles;* John Wiley & Sons: New York, NY, 1983; p. 72.
8. Salzman, G. C. In *Cell Analysis;* Catsimpoolas, N., Ed.; Plenum Publishing Co.: New York, New York, 1982; Vol. 1; pp. 111-143.
9. Kogelnik, H.; Li, T. *Appl. Opt.* **1966,** *5,* pp. 1550-1567.
10. Ashkin, A.; Dziedzic, J. M. *Appl. Phys. Lett.* **1974,** *24,* pp. 586-588.
11. Buican, T. N.; Neagley, D. L.; Morrison, W. C.; Upham, B. D. In *New Techniques in Cytometry;* Salzman, G. C., Ed.; Proceedings of SPIE; SPIE: Bellingham, Washington, 1989, Vol. 1063; pp. 190-197.
12. Visscher, K.; Brakenhoff, G. J. *Cytometry* **1990,** Supplement *4,* p. 17.
13. Horn, B. K. P. *Robot Vision;* The MIT Electrical Engineering and Computer Science Series; MIT Press, Cambridge, MA, 1986.
14. Moravec, H.P. *Obstacle Avoidance and Navigation in the Real World by a Seeing Robot Rover;* Ph.D. dissertation; Stanford University, Palo Alto, CA, 1980.

RECEIVED April 15, 1991